

# Use of Spherical Nanoindentation Protocols to Study the Anisotropic Mechanical Response of Alpha-Beta Single Colonies in Ti-6Al-4V Alloy



SOUMYA MOHAN, ADAM L. PILCHAK, and SURYA R. KALIDINDI

The recently developed spherical nanoindentation stress-strain protocols were employed in this study to investigate systematically the anisotropic elastic and yield response of the individual  $\alpha$ - $\beta$  colonies in a Ti-6Al-4V alloy. This was accomplished by indenting selected individual colonies with different lattice orientations of the secondary  $\alpha$  in the colony (measured by electron back-scattered diffraction) in the polycrystalline sample. It is seen that the employed protocols can provide reliable and consistent information on the elastic-plastic anisotropy of the colonies in a high-throughput manner, compared to the other approaches being explored in current literature. Furthermore, the responses measured in this study have been compared against similar measurements on differently oriented grains of primary  $\alpha$  in another Ti-6Al-4V sample. It was noted that the  $\alpha$ - $\beta$  colonies exhibit distinctly different elastic and plastic anisotropy compared to the primary  $\alpha$  grains. Specifically, a significant dip in the indentation yield properties at 45 degrees declination angle (between  $\bar{c}$  axis of colony  $\alpha$  and the indentation direction) was observed, while the elastic response was found to be mostly isotropic. The experimental protocols presented in this work are broadly applicable to other grain-scale morphologies and alloys, and the results produced from these protocols will be invaluable to the further development and refinement of mesoscale material constitutive models.

<https://doi.org/10.1007/s11661-024-07419-3>

© The Minerals, Metals & Materials Society and ASM International 2024

## I. INTRODUCTION

TITANIUM alpha-beta ( $\alpha$ - $\beta$ ) alloys are widely used in aerospace components and petrochemical plants due to their superior properties such as high strength to weight ratio, corrosion resistance, creep resistance, and fatigue properties.<sup>[1-8]</sup> The rich diversity of phases and their morphologies at different microstructure length scales offer tremendous promise for modulating their effective (macroscale) properties with relatively simple thermomechanical processing steps.<sup>[3,9]</sup> Specifically, the bimodal structures containing both primary  $\alpha$  (globular morphology) and colony microstructures (secondary  $\alpha$ -retained  $\beta$  lamellar morphology) offer tremendous potential for various aerospace applications.<sup>[1,2,10]</sup> The systematic quantification of grain-scale elastic and plastic anisotropy for primary  $\alpha$  as well as colony  $\alpha$ - $\beta$

is essential for the rational design and development of new alloys with better overall mechanical properties.

Crystal plasticity (CP) models are typically used to model the grain-scale anisotropic response of  $\alpha$ - $\beta$  microstructures.<sup>[11-22]</sup> Reliable estimates of the grain-scale properties such as single crystal elastic constants, critical resolved shear strengths (CRSS) and slip hardening exponents are needed as inputs for these models.<sup>[12,13,16,18,19,21,22]</sup> In contrast to primary  $\alpha$ , whose elastic and plastic anisotropy as a function of orientation and chemical composition has been studied extensively in literature,<sup>[23-33]</sup> there is limited understanding of the elastic-plastic anisotropy at the individual  $\alpha$ - $\beta$  colony level<sup>[14-16,18,20]</sup> even at room temperature. For example, estimates for the relative strengths of the different slip families in primary  $\alpha$  grains of different compositions have been reported in prior literature,<sup>[34-36]</sup> but not for colony  $\alpha$ - $\beta$  grains. Current CP simulations often make assumptions that simplify greatly the effective (homogenized) anisotropic properties of single colonies,<sup>[16-19]</sup> without any supporting experimental evidence. Moreover, they typically calibrate the grain-scale CP model parameters to available experimental data at the polycrystal scale.<sup>[20]</sup> Alternately, simplifying assumptions are often made about whether the colonies are stiffer and/or harder than the primary  $\alpha$  grains of the same lattice orientation in the same alloy. For example, Bridier

SOUMYA MOHAN and SURYA R. KALIDINDI are with the Woodruff School of Mechanical Engineering, Georgia Institute of Technology, Atlanta GA, 30318. Contact e-mail: surya.kalidindi@me.gatech.edu ADAM L. PILCHAK is with the Pratt & Whitney, 400 Main Street, East Hartford, CT 06118.

Manuscript submitted February 1, 2024; accepted April 18, 2024.

*et al.*<sup>[21]</sup> assumed the effective strength of colonies to be 1.25 times that of primary  $\alpha$  grains in their models to incorporate a Hall–Petch type strengthening effect from the secondary  $\alpha$ -retained  $\beta$  interfaces. Other approaches have directly estimated experimentally the effective tensile properties of the retained  $\beta$  from macroscale measurements on alloys of different phase fractions but same phase compositions. For example, it was estimated that the retained  $\beta$  in Ti–Mn alloys<sup>[37]</sup> was approximately 3 times stronger than the secondary  $\alpha$  phase. Although these approaches provide a rough order-of-magnitude estimates, they are not adequate for supporting rational materials design efforts, because of the high uncertainty associated with these estimates due to changes in composition, phase fractions, *etc.*

Colony  $\alpha$ - $\beta$  comprises of alternating ductile  $\alpha$  and retained ‘parent’  $\beta$  phases with lamellar morphologies, with the two phases following the Burgers orientation relationship (BOR), *i.e.*,  $(0001)_\alpha \parallel (110)_\beta$ , and  $[11\bar{2}0]_\alpha \parallel [1\bar{1}1]_\beta$ . Additionally, the  $\alpha$ - $\beta$  interface is nearly parallel to the  $(\bar{1}100)_\alpha$  and  $(112)_\beta$  which is close to  $\langle 7\bar{5}20 \rangle \parallel \langle 335 \rangle$  which is  $\sim 14.4$  deg away from  $[11\bar{2}0]_\alpha \parallel [1\bar{1}1]_\beta$  in the  $(110)_\beta$  plane.<sup>[38–42]</sup> The relevant slip systems for  $\alpha$  include the prismatic and basal slip planes with  $\langle \bar{a}_1 \rangle$ ,  $\langle \bar{a}_2 \rangle$ , and  $\langle \bar{a}_3 \rangle$  slip directions, and first- and second-order pyramidal and pyramidal slip planes with  $\langle \bar{c} + \bar{a} \rangle$  slip directions. Earlier macroscale studies (uniaxial tensile tests, creep tests)<sup>[43–45]</sup> suggested easy slip transfer between  $\alpha$ - $\beta$  interfaces due to the BOR, with colony size being an important length scale influencing the yield and creep properties.<sup>[9]</sup> Several additional factors may impact colony slip strengths, including  $\alpha$ - $\beta$  interfaces as well as the relative strengths and compositions of  $\alpha$  and  $\beta$ . Quantitative understanding of the effects listed above is fairly limited at the current time, mainly because of the lack of adequate experimental data at the colony-scale. Prior attempts to quantify the elastic-plastic response of single  $\alpha$ - $\beta$  colonies (with a unique  $\alpha$  orientation) primarily included small scale mechanical compression/tension tests, and characterizing slip transmission through the  $\alpha$ - $\beta$  interface using electron microscopy. Summarily, such studies have generally reported large anisotropy in the values of CRSS for different slip families (prismatic, basal, pyramidal), *e.g.*, 236–446 MPa for Ti–8Al–1Mo–1V (Ti-811),<sup>[46]</sup> 330–709 MPa for Ti–6Al–4V (Ti-6-4).<sup>[47]</sup> Smaller but non-negligible differences were reported for the CRSS values for the slip systems within the same slip family, *e.g.*, between prism  $\langle \bar{a}_1 \rangle$  (262.5 MPa) and prism  $\langle \bar{a}_2 \rangle$  (292.5 MPa) from compression on Ti–5Al–2.5Sn–0.5Fe (Ti-5-2.5).<sup>[38]</sup> Values of 376–453 MPa were reported for prismatic slip strengths for  $\langle \bar{a}_1 \rangle$ ,  $\langle \bar{a}_2 \rangle$ ,  $\langle \bar{a}_3 \rangle$ , and 341–366 MPa for basal slip strengths for  $\langle \bar{a}_1 \rangle$ ,  $\langle \bar{a}_2 \rangle$ ,  $\langle \bar{a}_3 \rangle$  from compression on Ti-6-4.<sup>[48]</sup> Similarly, values of 330–405 MPa were reported for basal slip strengths for  $\langle \bar{a}_1 \rangle$ ,  $\langle \bar{a}_2 \rangle$ ,  $\langle \bar{a}_3 \rangle$  from compression on Ti6Al–2Sn–4Zr–2Mo (Ti-6242)<sup>[49]</sup> and 260–300 MPa for basal slip strengths for  $\langle \bar{a}_1 \rangle$ ,  $\langle \bar{a}_2 \rangle$ ,  $\langle \bar{a}_3 \rangle$  from tension on Ti-6242.<sup>[50]</sup>

Chan *et al.*<sup>[46]</sup> performed compression tests on Ti-811 across a range of colony  $\alpha$  orientations, thereby varying

the inclination in the  $\alpha$ - $\beta$  interface; and found that the CRSS increased as the active slip direction (from optically observed macroscopic slip) approached perpendicularity to the  $\alpha$ - $\beta$  interface. Similar observations were reported by Suri *et al.*,<sup>[38]</sup> where the CRSS value was found to be higher for prismatic slip in Ti-5-2.5 for  $\langle \bar{a}_2 \rangle$ , than for  $\langle \bar{a}_1 \rangle$ , with the former being closer to the normal to the  $\alpha$ - $\beta$  interface in their compression tests. However, the models proposed in these studies were quite different. Chan *et al.* proposed that the larger CRSS for slip approaching normality to the interface implied a length scale effect, *i.e.*, the smaller ‘slip length’ in the secondary  $\alpha$  is attributed to a Hall–Petch type strengthening. On the other hand, Suri *et al.* proposed a geometric model for slip transmission, with the underlying assumption being that the slightly longer burgers length for  $\alpha$  and the change in direction would lead to formation of a higher residual dislocation content at the interface. This geometric model was also able to rationalize the observed slip behavior for basal  $\langle \bar{a}_1 \rangle$ ,  $\langle \bar{a}_2 \rangle$ , and  $\langle \bar{a}_3 \rangle$  slip in Ti-6242 single colonies for compression tests conducted by Savage *et al.*<sup>[50]</sup> Suri *et al.* concluded that a Hall–Petch type strengthening overestimated the experimental differences in CRSS. Both Chan<sup>[46]</sup> and Suri<sup>[38]</sup> assumed that  $\alpha$  is the softer phase, since slip initiated there, but the experimental evidence for this assertion is not clear. Savage *et al.*<sup>[49]</sup> compared the CRSS values of the prismatic and basal slip systems by conducting micro-tensile tests on Ti-6242 colonies, and reported that prism  $\langle \bar{a}_1 \rangle$  slip was the easiest slip. Contrarily, Htwe *et al.*<sup>[48]</sup> found that CRSS for basal slip was lower than that of prismatic slip from their micro-tensile tests on single colony Ti-6-4; they proposed that the BOR between  $\alpha$ - $\beta$  leads to the interface acting as a slip pile-up type barrier for prismatic slip, whereas a pinning model was proposed for basal slip. However, no experimental evidence for the pinning/pile up model was provided.

There are only few studies investigating pyramidal  $\langle \bar{c} + \bar{a} \rangle$  slip in single colonies in Ti alloys. Ding *et al.*<sup>[29,51]</sup> used cantilever tests for Ti-6-4 and reported evidence of  $\langle \bar{c} + \bar{a} \rangle$  slip transfer across the  $\alpha$ - $\beta$  interface in tension. Mine *et al.*<sup>[47]</sup> compared the responses of primary  $\alpha$  and colony  $\alpha$ - $\beta$  phases in Ti-6-4, and concluded that  $\beta$  reduced the CRSS of  $\langle \bar{c} + \bar{a} \rangle$  slip in the colony phase, and increased the CRSS in basal and prismatic slips, resulting in a decrease in anisotropy compared to primary  $\alpha$ . Additionally, CRSS for a slip system was found to increase with the fraction of total  $\beta$  length along the slip direction (the product of the effective  $\beta$  length and the frequency of intersecting  $\beta$ ). In addition to a report on the dwell fatigue of Ti-6242,<sup>[52]</sup> where a comparison was made between primary  $\alpha$  Ti–6Al, and colony Ti-6242, to the best of our knowledge, these were the only reported works on single colonies that compared CRSS values of primary  $\alpha$  to colony  $\alpha$ - $\beta$ , as well as reported CRSS for  $\langle \bar{c} + \bar{a} \rangle$  slip. In tensile tests at 20 K on Ti-6-4 duplex microstructure powder metallurgy samples, prismatic slip was reported to dominate primary  $\alpha$ , whereas basal slip was dominant in the colony grains.<sup>[53]</sup>

It is clear from the above discussion that there are differences in the reported values of the CRSS for the different slip systems in  $\alpha$ - $\beta$  colonies as well as competing theories of slip transmission and effective strengths of the colonies. The central impediment in advancing our understanding of these microscale phenomena comes from the lack of sufficient and reliable data. This is mainly because the microscale experiments (tension or compression tests) are effort intensive and require sophisticated equipment and significant expertise (for sample preparation, proper alignment and loading of samples, *etc.*). Although it is possible to produce large single colony samples, this option becomes cumbersome for testing a multitude of alloy compositions.

Instrumented indentation tests offer an excellent high-throughput avenue that addresses many of the challenges described above. Historically, sharp nanoindenters have been used to study the mechanical properties of the constituent phases in bimodal microstructures. For example, differences in relative nano-hardness between primary  $\alpha$  and colony  $\alpha$ - $\beta$  were observed in bimodal samples.<sup>[54,55]</sup> Interestingly, these studies revealed a lower hardness of the  $\alpha$ - $\beta$  colonies compared to primary  $\alpha$ , which was attributed to elemental partitioning of Al, which is a strong substitutional solid solution strengthener, between the two phases. Indeed, as the Al wt pct gap decreases, the hardness of primary  $\alpha$  and colony  $\alpha$ - $\beta$  approach each other.<sup>[54]</sup> However, the measured hardness values in these tests cannot be easily converted to CRSS values. Recently developed spherical indentation stress-strain measurement and analyses protocols<sup>[56,57]</sup> address this limitation. These protocols use instrumented load-displacement curves and convert them to indentation stress-strain responses. The viability of these protocols for estimating grain-scale intrinsic elastic and plastic properties was successfully demonstrated using finite element simulations for a number of single-phase cubic metals<sup>[58,59]</sup> and primary  $\alpha$  in Ti alloys,<sup>[24,25]</sup> as well as recently for colony Ti alloys based on the results presented in this work.<sup>[14,15]</sup>

In this paper, we will extend and explore the recently developed spherical indentation protocols to analyze the effective grain-scale mechanical response of colonies in a Ti-6-4 alloy. Specifically, the elastic and yield responses of colonies will be evaluated as a function of the declination angle of the secondary  $\alpha$ . Additionally, the response will be compared to corresponding measurements conducted previously on primary  $\alpha$  for the same alloy.<sup>[24,25]</sup> We observed a significant reduction in the indentation yield strength at a declination angle of 45 deg, and a lower elastic anisotropy. These results are presented and discussed in this paper.

## II. MATERIALS AND METHODS

### A. Materials and Sample Preparation

An adequately large sample of Ti-6-4 was obtained from AFRL (Wright-Patterson Air Force Base, Ohio), with an alloy composition summarized in Table I. The

**Table I. Compositions for Colony  $\alpha$ - $\beta$  Studied Here, and the Primary  $\alpha$  in the Ti-6-4 sample<sup>[24,25]</sup>**

Composition (Wt Pct)	Al	V	Fe	O
Colony $\alpha$ + $\beta$ Ti-6Al-4 V	6.3	4.17	0.2	0.18
Primary $\alpha$ Ti-6Al-4V	7.04	1.62	—	0.20

The colony composition is the average composition of the Ti-6-4 alloy sample, and the primary composition is the local phase composition that was measured using electron probe microanalysis (EPMA) in Ref. [7]. The average composition of the program material is assumed to be the same as the colony composition, since the microstructure was nearly 100 pct colony.

as-received material was  $\beta$ -annealed at 1050 °C for 2 hours, then air cooled in vermiculite to get a  $\sim$ 100 pct colony microstructure. Stabilizing heat treatment was performed at 700 °C for 4 hours to fully relax any residual stresses. The sample was cold mounted and prepared for indentation and microstructure characterization. Grinding steps (800, 1200 grit) and polishing steps (9, 3 and 1  $\mu$ m) were performed to ensure that the surface to be indented was free of any damaged layers. Final chemo-mechanical polishing was performed using Vibromet<sup>®</sup>, using a solution of 0.05 micrometer colloidal silica, hydrogen peroxide and water in 1:1:5 ratio, respectively, for 8–10 hours.

### B. Spherical Indentation Tests

Spherical nanoindentation measurements and analyses protocols developed by Kalidindi and Pathak<sup>[56,57]</sup> (described in detail in Section II-C) were employed. Orientation imaging microscopy (OIM) was performed with a Tescan Mira Field Emission-Scanning Electron Microscope (FE-SEM) to identify the colonies where the indentations were to be performed. The goal is to identify and indent colonies exhibiting different declination angles (angle between the  $\langle\bar{c}\rangle$ -axis of the grain and the indentation direction). In grain-scale indentations, where the grain orientation is represented by Bunge angles ( $\phi_1$ ,  $\phi$ ,  $\phi_2$ ),<sup>[60]</sup> spherical indentation measurements are insensitive to the angle  $\phi_1$  (this represents a sample rotation around the indentation direction). The angle  $\phi$  is the declination angle described earlier, with a 0 deg declination angle implying that the indentation is performed parallel to the  $\langle\bar{c}\rangle$  axis of the hcp crystal. Similarly, a 90 deg declination angle implies that the indentation is performed perpendicular to the  $\langle\bar{c}\rangle$ -axis of the hcp crystal. Generally, for hcp crystals,  $\phi_2$  has not been observed to have a significant influence on the measured indentation properties and has been attributed to the high transverse symmetry of the hcp phase.<sup>[24,25]</sup> However, this is not necessarily the case for the present work because the effective mechanical response of the colonies is not expected to exhibit this symmetry. Our analyses in this paper utilized only the  $\alpha$  orientations were measured in this study. In a more detailed future study, one might also measure the  $\beta$  orientations and examine their role. In the present study, we are implicitly assuming that the BOR defines the relationship between the  $\alpha$  and  $\beta$  orientations in each colony.



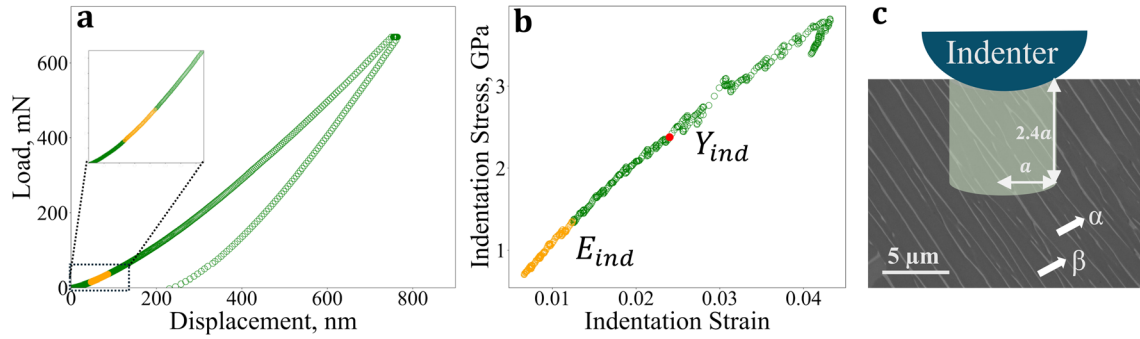


Fig. 1—(a) Example measured indentation load–displacement curve from a single colony. The orange segments in the figure were selected for the elastic analyses using Hertz’s theory. (b) Corresponding indentation stress–strain curve. (c) Schematic description of the estimated effective indentation zone at yield in the experiments reported in this work (Color figure online).

Keysight G200 Nanoindenter (formerly Agilent) was used to conduct the spherical indentations reported in this paper. The indentations were performed near grain centers, away from colony boundaries, using an indenter tip of radius,  $R_i = 100\mu\text{m}$ . Previous work on Ti-6-4 alloys<sup>[24,25]</sup> with the same indenter tip showed a contact radius at yield of  $\sim 3.5\mu\text{m}$ . For our sample, the grain sizes ranged from 35 to 45  $\mu\text{m}$ , and the colony  $\alpha$  lath size ranged from 1 to 1.3  $\mu\text{m}$ . Hence, the measurements with the selected indenter are assumed to correspond to the effective response from multiple lamellae. Larger colonies were selected for the indentations to minimize the effects of the neighboring colonies on our measurements. The indentations were performed to a total depth of 800 nm at a constant strain rate (defined as loading rate/load) of  $0.05\text{ s}^{-1}$ . The test protocol included a continuous stiffness measurement (CSM), which superimposes the monotonic loading signal with harmonic oscillations. The displacement amplitude for CSM was kept at 2 nm with a frequency of 45 Hz.<sup>[61]</sup>

### C. Spherical Indentation Stress–Strain Protocols

The spherical indentation stress–strain protocols used in this work have been described extensively in prior literature.<sup>[56,57,62]</sup> These protocols utilize the following definitions of indentation stress ( $\sigma_{\text{ind}}$ ) and indentation strain ( $\epsilon_{\text{ind}}$ )<sup>[56]</sup> to extract the indentation stress–strain (ISS) curves from the measured indentation load–displacement (*i.e.*,  $P$ – $h$ ) curves (as shown in Figure 1(a)):

$$\sigma_{\text{ind}} = \frac{P}{\pi a^2} \quad [1]$$

$$\epsilon_{\text{ind}} = \frac{4}{3\pi} \frac{h}{a} \quad [2]$$

where  $a$  is the contact radius under load. In these protocols, the contact radius is estimated from the use of Hertz’s theory<sup>[63]</sup> on the measured CSM signal (denoted by  $S$ ) and the effective stiffness  $E_{\text{eff}}$  as

$$a = \frac{S}{2E_{\text{eff}}} \quad [3]$$

Overall, the analysis protocols comprise the following main steps<sup>[56]</sup>:

- (1) Perform “zero-point” corrections on the raw load–displacement curves to account for some of the unavoidable effects occurring in the initial contact<sup>[56]</sup> (of the order of a few nanometers) such as those due to surface roughness.<sup>[64]</sup>
- (2) Following the protocols described in prior work, estimate the effective indentation modulus,  $E_{\text{eff}}$ , from the corrected load–displacement data by fitting the initial elastic portion to Hertz’s theory.<sup>[63]</sup> This step involves selection of an initial elastic segment from the corrected load–displacement response. It is important to ensure that the selected initial elastic regime corresponds to the composite response of secondary  $\alpha$  and parent  $\beta$ , *i.e.*, the estimated indented volume for the selected region comprises at least 3–4 lamellae. Figure 1(c) depicts schematically the evolving primary indentation zone as a cylinder of radius  $a$  and height of  $2.4a$ . Note that the primary indentation zone in the early part of the load–displacement data (corresponding to the first few 10 s of nms.) most likely includes only one phase or one lamella. Only as the indentation depth increases, the measured response corresponds to the effective colony response. For all the tests reported in this work, it was ensured that the value of the  $E_{\text{eff}}$  is estimated from a segment of the initial elastic response that corresponded to a sufficiently large, indented volume.
- (3) Compute the ISS curve from the corrected load–displacement curve using Eqs. [1], [2], and [3] (see Figure 1(b)).
- (4) Estimate the indentation modulus,  $E_{\text{ind}}$ , as the slope of the initial elastic regime in the ISS curve (see Figure 1(b)), and indentation yield strength,  $Y_{\text{ind}}$ , as corresponding to a 0.002 indentation plastic strain offset on the ISS curve (see Figure 1(b)).
- (5) Document the variance in the estimated values of  $E_{\text{ind}}$  and  $Y_{\text{ind}}$  to reflect the uncertainty arising from the analyses protocols.<sup>[61]</sup>

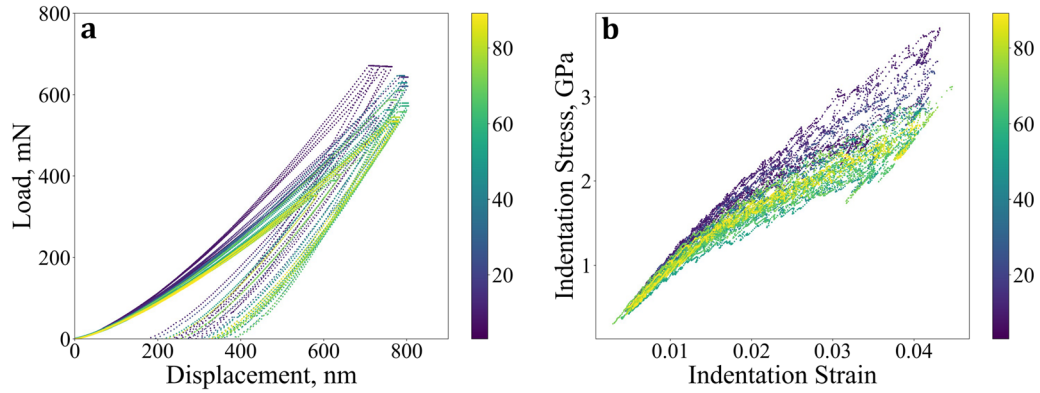


Fig. 2—(a) Measured load–displacement curves for colonies with varying declination angles. The legend on the right identifies the declination angles. (b) Analyzed indentation stress strain curves for colonies with varying declination angles. The legend on the right identifies the declination angles.

### III. RESULTS AND DISCUSSION

Figure 2(a) shows raw data for 34 indentation load–displacement curves for colony Ti-6-4, color graded corresponding to the declination angles in the range 3.1 to 89.2 deg, with the lighter green representing the larger angles and dark blue the smaller angles. Summarily, the protocols offer a faster, high throughput method of evaluating small scale elastic-plastic behavior, since large amounts of data can be collected from a small volume of sample, within a significantly reduced time compared to single colony micro tensile/compression tests. All the indentation data in Figure 2 was collected from  $< 5 \text{ cm}^2$  surface area. Conservatively, ample data can be collected in about a week from each sample, this includes sample preparation, EBSD analysis and  $\sim 50$  indentation tests. The indentation analysis itself can take up to a week per sample (done manually using a macro program). In contrast, micro tensile/compression tests can take 6 months to 1 year to gather data from one material (typically 1–3 samples for each slip family).

There are some drawbacks to evaluating properties using spherical indentation protocols. Since the imposed stress-state is largely in compression, it cannot provide any insights into possible tension-compression asymmetry in the response of the individual colonies, which is typically observed in Ti alloys.<sup>[33,50,65,66]</sup> Furthermore, the protocols are critically dependent on good sample preparation. This is because the protocols rely on a good estimation of the effective indentation modulus from the initial elastic response, which is associated with very small indentation zone sizes. The biggest uncertainty in the results from the spherical indentation protocols employed here comes from lack of knowledge about how far the indented grain extends underneath the sample surface (in the indentation direction). This is important because the presence of a differently oriented grain underneath the indented surface can significantly influence the measurements. Selecting larger colonies can help mitigate this, however they may not always be available. Despite these concerns, the indentation tests are better able to reveal important insights into the

colony-scale response, primarily because of their high reproducibility and their ability to conduct many tests that can be analyzed in a rigorous statistical framework.

A clear trend is observed from Figure 2(a), indicating anisotropy in the colony-scale load–displacement response as a function of declination angles. The  $P$ – $h$  data shows a stiffer and harder response with lower declination angles (indentation direction closer to  $\langle \vec{c} \rangle$ ). The differences in the  $P$ – $h$  responses in the range of 45 to 90 deg declination angles are not very significant. A much more detailed analyses of the relationship between the measured elastic and plastic response to the colony orientation is presented next. This data is available in the NIST materials data repository.<sup>[67]</sup>

#### A. Elastic Indentation Properties of Colony $\alpha$ - $\beta$ Compared to Primary $\alpha$

Figure 3 summarizes the measured elastic indentation moduli of the composite colony  $\alpha$ - $\beta$  as a function of the declination angle in the secondary  $\alpha$  in the colony. These measurements are compared against the measurements from primary  $\alpha$  grains from two similar samples studied extensively in prior studies.<sup>[24,25]</sup> Note that the colony grains were studied here using a different indenter tip radius (100  $\mu\text{m}$  tip radius for this work compared to a tip radius of 15.2  $\mu\text{m}$  used in the prior work on primary  $\alpha$ ). The larger indenter tip radius was necessary for the present study to ensure that we are measuring the bulk elastic-plastic response of the composite colony  $\alpha$ - $\beta$ . The conversion of the raw load–displacement curves into the normalized indentation stress–strain curves allows the comparison of the measurements obtained using the different indenter tip radii. As already noted, because of the loss of transverse symmetry in the effective response of colonies, the effective indentation modulus of the colony grains is expected to vary with  $\phi_2$ . However, the data in Figure 3 is plotted only with respect to  $\phi$  (representing angle to  $\vec{c}$  direction).

Figure 3 shows that  $E_{\text{ind}}$  for colony  $\alpha$ - $\beta$  shows a lower elastic anisotropy compared to the primary  $\alpha$ . The difference between  $E_{\text{ind}}$  for colony  $\alpha$ - $\beta$  and primary  $\alpha$  is quite pronounced for  $\phi < 10$  deg; this difference is

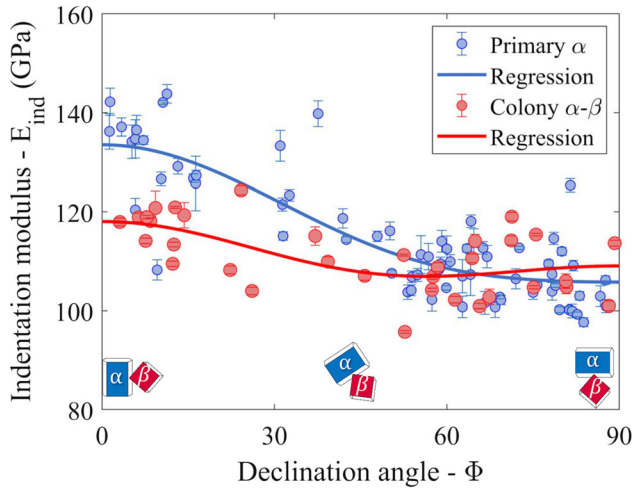


Fig. 3—Variation of the indentation modulus of primary  $\alpha$  and colony  $\alpha$ - $\beta$  in Ti-6-4 as a function of the declination angle. The solid lines represent trendlines.

**Table II. Summary of the Measurements of  $E_{\text{ind}}$  for Primary  $\alpha$  and Colony  $\alpha$ - $\beta$  in Two Intervals of Declination Angles**

Sample	$E_{\text{ind}}, \phi < 10^\circ$	$E_{\text{ind}}, \phi > 60^\circ$
Colony $\alpha$ - $\beta$	$118.11 \pm 2.22$	$108.42 \pm 6.04$
Primary $\alpha$	$135.74 \pm 5.12$	$106.23 \pm 5.54$

quantified in Table II, where  $E_{\text{ind}}$  for colony microstructure is found to be 13 pct lower than that for primary  $\alpha$ . This indicates that retained  $\beta$  makes the composite colony more compliant at low declination angles (*i.e.*,  $\phi < 10$  deg). The results also imply that the effect of the retained  $\beta$  on the effective colony modulus is significantly less at larger declination angles ( $\phi > 60$  deg, shown in Table II). The decrease in  $E_{\text{ind}}$  with increasing declination angle for primary  $\alpha$  has been previously attributed to  $\vec{c}$  being the stiffest direction.<sup>[24,25,68,69]</sup>

To explain the observed elastic anisotropic response of the colony  $\alpha$ - $\beta$ , it is important to review the orientations of both  $\alpha$  and  $\beta$  in the colonies with the changes in the  $\alpha$  declination angles. These are shown schematically along the  $x$ -axis in Figure 3. Since the  $\alpha$ - $\beta$  interface is very close ( $\sim 15^\circ$ ) to the prismatic plane,<sup>[38]</sup> at the declination angle of 0 deg, based on the BOR ( $[11\bar{2}0]_\alpha \parallel [1\bar{1}1]_\beta$ ), the relevant direction for retained  $\beta$  that is parallel to indentation direction as well as  $\vec{c}$  of secondary (colony)  $\alpha$  would be  $[101]$ . This has also been confirmed in prior literature.<sup>[38–42]</sup> The unique identification of the cubic crystal direction parallel to the indentation direction is only possible for the zero declination angle. For non-zero declination angles, the indentation direction for the bcc component cannot be identified uniquely, as it can be any direction on a specified plane. For example, at 90 deg declination angle,  $[001]$ ,  $[110]$ , as well as  $[1\bar{1}1]$  directions are possible to be parallel to indenting direction.

Elastic anisotropy in cubic crystal is often characterized using the Zener anisotropy ratio. This ratio (denoted as  $A$ ) is very sensitive to the  $\beta$  compositions, which is estimated to be rich in V and lean in Al. Prior experimental and modeling literature on Ti-V compositions for  $\beta$  have estimate the range of  $A$  to be between 1 and 5.<sup>[26,70–73]</sup> Since  $A > 1$ , the elastic anisotropy is expected such that the  $[111]$  direction would be the stiffest direction, while  $[100]$  direction would be the most compliant. The  $[110]$  direction is expected to be stiffer than  $[100]$  direction, but significantly more compliant compared to the  $[111]$  direction (especially for high  $A$  values). As the declination angle increases from 0 deg, it is seen that the cubic crystal direction parallel to the indentation changes from the  $[110]$  direction and gets close to  $[100]$  directions at intermediate declination angles. At the highest declination angles, the cubic crystal direction includes many of the orientations close to  $[111]$ . As a result, the contribution of beta to the measured modulus is expected to decrease a little up to moderate declination angles, but it should increase significantly at the highest declination angles. This provides a qualitative explanation for the observed differences in the trendlines seen in Figure 3 for the indentation moduli of primary and colony  $\alpha$  as a function of the declination angle. Overall, this also explains the reduction in elastic anisotropy observed for colony  $\alpha$ - $\beta$  compared to primary  $\alpha$ .

## B. Indentation Yield Strengths of Colony $\alpha$ - $\beta$ and Primary $\alpha$

Figure 2(b) shows the indentation stress strain curves for all the declination angles. From the measured load displacement curves (Figure 2(a)), it is seen that the samples are generally depicting softer responses with increases in the declination angles. The trends however are not clear from the load–displacement curves, especially for the larger declination angles. In our protocols, converting the load–displacement curves to indentation stress–strain curves (see Figure 2(b)) allows us to study these relationships in a much more quantitative manner.

Figure 4 summarizes the measurements of  $Y_{\text{ind}}$  for both primary  $\alpha$  (from prior studies)<sup>[24,25]</sup> and the colony  $\alpha$ - $\beta$  (this study) as a function of declination angle. The measured value of  $Y_{\text{ind}}$  for colony  $\alpha$ - $\beta$  is consistently lower than that of primary  $\alpha$ . This is in contrast to assumptions made in some modeling studies in the literature, *viz.*<sup>[19,21]</sup> It has been generally presumed that  $\alpha$ - $\beta$  interfaces provided significant Hall–Petch strengthening which would lead to increased CRSS in the colonies. However, the measurements presented in Figure 4 clearly suggest that there is a significant softening effect from the presence of  $\beta$ , therefore, retained  $\beta$  is most likely to be softer than primary  $\alpha$  in the sample studied here.

Chemical composition is expected to play a significant role in controlling the responses of both the primary  $\alpha$  and the colony  $\alpha$ - $\beta$ . Specifically, Al, O, and C strengthen the  $\alpha$  phase, while V and Fe strengthen the  $\beta$  phase in Ti-6Al-4V.<sup>[1]</sup> The effect of composition on the indentation yield strength was quantified in a recent study,<sup>[25]</sup> where the same spherical indentation protocols described in this



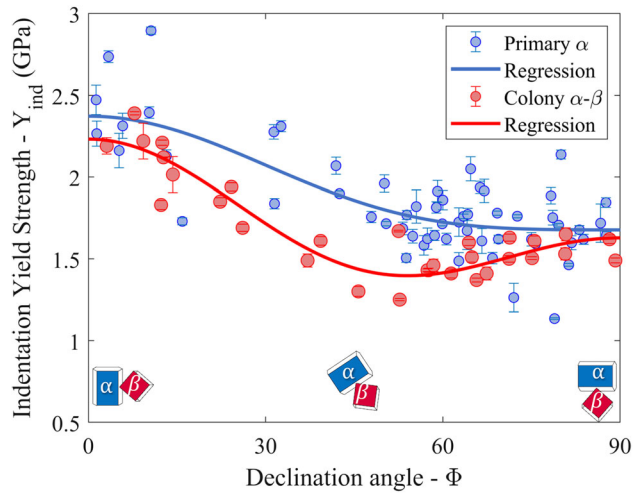


Fig. 4—Indentation yield strength of primary  $\alpha$  in Ti-6-4 and colony  $\alpha$ - $\beta$  in Ti-6-4 alloy as a function of declination angle. The solid lines are trendlines.

paper were employed. Specifically, it was reported that the  $Y_{ind}$  values of primary  $\alpha$  showed a significant correlation to the Al and Mo equivalence.<sup>[74]</sup> The composition of secondary  $\alpha$  was not measured in this study, but an estimate of the composition for the same was determined from thermodynamic equilibrium calculations using ThermoCalc software. As explained in Table I, the average composition of the sample in this study is assumed to be the colony composition since it contains almost 100 pct colony phases. For the volume fraction of retained  $\beta$  estimated for colony Ti-6-4 ( $12.2 \pm 2.1$  pct from related work),<sup>[15]</sup> and using the colony composition of the alloy in Table I, the corresponding Al wt pct for secondary  $\alpha$  is 6.66. This 0.4 wt pct change in Al is one of the contributions to the difference in  $Y_{ind}$  in primary  $\alpha$  and colony  $\alpha$ - $\beta$ . Clearly, more detailed experimental studies are needed to precisely understand the effect of the change in composition of secondary  $\alpha$  compared to the primary  $\alpha$  in bimodal microstructures. Such investigations should also systematically interrogate different secondary  $\alpha$  morphologies (basketweave vs lamellar colony) and lath thicknesses.

The softening effect of  $\beta$  observed in Figure 4 is likely to reduce significantly with a decrease in the  $\beta$  volume fraction. Similarly, the strengthening effect of the  $\alpha$ - $\beta$  interfaces is likely to be promoted by a decrease in  $\alpha$  thickness. It should be noted that since the strength of  $\beta$  phase is very sensitive to compositions,<sup>[26]</sup> this observation of a softer  $\beta$  might change with a different alloy composition. Therefore, it is very likely that response of the colonies seen in Figure 4 will change dramatically with changes in  $\beta$  morphology, volume fraction and composition. Effect of  $\beta$  volume fraction on critical resolved shear strengths was observed in previous work as well<sup>[47,48]</sup> The softer  $\beta$  inferred from our study deviates from previous work in Ti-Mn alloys, where  $\beta$  was 3 times stronger.<sup>[37]</sup> This could be because the Mn alloying element would segregate preferentially to and strengthen the  $\beta$ . In general, it should be expected that smaller  $\beta$  volume fractions and smaller  $\beta$  thickness per volume of material will increase the effective yield strength of the colony.

Figure 4 also indicates a pronounced dip in the indentation yield strength for colony  $\alpha$ - $\beta$  near a declination angle ( $\phi$ ) of 45 deg, followed by a slight increase in the indentation yield strength values at a declination angle ( $\phi$ ) of 90 deg. This trend is quite distinct from the corresponding trend for primary  $\alpha$ , which exhibited a much steadier decrease. This dip has also been reported in CPFEM simulations of spherical indentations in colony  $\alpha$ - $\beta$  work,<sup>[14]</sup> and has been attributed to the orientation softening of  $\beta$ . In the FE simulations, this trough was observed to correspond to relatively high levels of slip activity in the softest bcc slip systems. In other words, in this test condition, the slip systems in the  $\beta$  are much more favorably oriented for slip, compared to the other test conditions, causing the discernible dip seen in the indentation yield. The fact that this dip occurs consistently in both numerical simulations and experiments attests to both their reliabilities. The dip offers further evidence that retained  $\beta$  is softer, because it is most active at that range of declination angle. Previous literature aligns with our observations as well. Yoji *et al.* and Mine *et al.* have both shown that the colony strength is lowest when basal slip was activated in the secondary  $\alpha$ <sup>[47,48]</sup> for micro-tensile tests. Additionally, Ambard<sup>[53]</sup> showed basal slip being favored in the colony phase in a bimodal polycrystalline Ti-6-4 alloy. Of course, a direct comparison between micro-tensile and the indentation data is not possible. One of the challenges with indentation measurements and analyses is using the indentation yield and elastic data to calculate grain-scale elastic-plastic material constants, such as critical resolved shear strengths (CRSS) and single crystal elastic constants. Recent advances in spherical indentation analyses protocols have reported significant progress in this direction.<sup>[14,58,59,75]</sup>

#### IV. CONCLUSIONS

The  $\alpha$ - $\beta$  colonies exhibit distinctly different elastic and plastic anisotropy compared to the primary  $\alpha$  grains. The composite elastic response was found to be more isotropic than the elastic anisotropy of primary  $\alpha$ . A significant dip in the indentation yield properties at 45 deg declination angle was observed. For the specific sample composition and microstructure studied in this work, the retained  $\beta$  is softer. Furthermore, the  $\beta$  regions experience the highest driving force for slip near 45 deg declination angle. FE simulations from related work<sup>[14]</sup> confirm these observations.

#### ACKNOWLEDGMENTS

The authors SK and SM would like to acknowledge the AFOSR Grant FA9550-18-1-0330 (Program manager, J. Tiley) for this work. We are grateful to Dr. Aditya Venkatraman for his assistance in calculating the indentation yield regressions and contour plots using spherical harmonics.

## CONFLICT OF INTEREST

The authors declare that they have no conflict of interest.

## REFERENCES

1. G. Lutjering and J.C. Williams: *Engineering* 2007, pp. 442–42.
2. D. Banerjee and J.C. Williams: *Acta Mater.*, 2013, vol. 61, pp. 844–79.
3. S. Banerjee and P. Mukhopadhyay: *Phase Transformations: Examples from Titanium and Zirconium Alloys*, Elsevier, Amsterdam, 2010.
4. C. Leyens and M. Peters: *Titanium and Titanium Alloys: Fundamentals and Applications*, Wiley, New York, 2006.
5. C. Veiga, J. Paulo Davim, and A.J.R. Loureiro: *Rev. Adv. Mater. Sci.*, 2012, vol. 32, pp. 133–48.
6. P. Pushp, S.M. Dasharath, and C. Arati: *Mater. Today*, 2022, vol. 54, pp. 537–42.
7. H.Y. Ma, J.C. Wang, P. Qin, Y.J. Liu, L.Y. Chen, L.Q. Wang, and L.C. Zhang: *J. Mater. Sci. Technol.*, 2024, vol. 183, pp. 32–62.
8. K. Li, J. Yang, Y. Yi, X. Liu, Y. Liu, L.-C. Zhang, W. Zhang, W. Li, D. Chen, and S. Zhou: *Acta Mater.*, 2023, vol. 256, p. 119112.
9. G. Lütjering: *Mater. Sci. Eng. A*, 1998, vol. 243, pp. 32–45.
10. R.R. Boyer: *Mater. Sci. Eng. A*, 1996, vol. 213, pp. 103–14.
11. S. Hémerly, A. Nait-Ali, and P. Villechaise: *Mech. Mater.*, 2017, vol. 109, pp. 1–10.
12. I.A. Riyad, W.G. Feather, E. Vasilev, R.A. Lebensohn, B.A. McWilliams, A.L. Pilchak, and M. Knezevic: *Acta Mater.*, 2021, vol. 203, p. 116502.
13. R. Ma, A.L. Pilchak, S.L. Semiatin, and T.J. Truster: *Int. J. Plast.*, 2018, vol. 107, pp. 189–206.
14. A. Venkatraman, D.L. McDowell, and S.R. Kalidindi: *Int. J. Plast.*, 2022, vol. 154, p. 103289.
15. A. Venkatraman, S. Mohan, R. Joseph, D.L. McDowell, and S.R. Kalidindi: *Modell. Simul. Mater. Sci. Eng.* 2023.
16. D. Deka, D.S. Joseph, S. Ghosh, and M.J. Mills: *Metall. Mater. Trans. A*, 2006, vol. 37A, pp. 1371–88.
17. J.R. Mayeur and D.L. McDowell: *Int. J. Plast.*, 2007, vol. 23, pp. 1457–85.
18. Y. Geng and N. Harrison: *Mater. Sci. Eng. A*, 2020, vol. 773, 138736.
19. G. Venkatramani, S. Ghosh, and M. Mills: *Acta Mater.*, 2007, vol. 55, pp. 3971–86.
20. Z. Zhang, T.-S. Jun, T.B. Britton, and F.P.E. Dunne: *J. Mech. Phys. Solids*, 2016, vol. 95, pp. 393–410.
21. F. Bridier, D.L. McDowell, P. Villechaise, and J. Mendez: *Int. J. Plast.*, 2009, vol. 25, pp. 1066–82.
22. P.J. Ashton, T.-S. Jun, Z. Zhang, T.B. Britton, A.M. Harte, S.B. Leen, and F.P.E. Dunne: *Int. J. Fatigue*, 2017, vol. 100, pp. 377–87.
23. J.S. Weaver and S.R. Kalidindi: *Mater. Des.*, 2016, vol. 111, pp. 463–72.
24. J.S. Weaver, M.W. Priddy, D.L. McDowell, and S.R. Kalidindi: *Acta Mater.*, 2016, vol. 117, pp. 23–34.
25. N. Millan-Espitia, S. Mohan, A.L. Pilchak, and S.R. Kalidindi: *Integr. Mater. Manuf. Innov.*, 2021, vol. 10, pp. 82–98.
26. S. Hémerly, P. Villechaise, and D. Banerjee: *Metall. Mater. Trans. A*, 2020, vol. 51A, pp. 4931–69.
27. J.C. Williams, R.G. Baggerly, and N.E. Paton: *Metall. Mater. Trans. A*, 2002, vol. 33A, pp. 837–50.
28. T.B. Britton, H. Liang, F.P.E. Dunne, and A.J. Wilkinson: *Proc. R. Soc. A*, 2010, vol. 466, pp. 695–719.
29. R. Ding, J. Gong, A.J. Wilkinson, and I.P. Jones: *Acta Mater.*, 2014, vol. 76, pp. 127–34.
30. R. Ding, J. Gong, A.J. Wilkinson, and I.P. Jones: *Philos. Mag.*, 2012, vol. 92, pp. 3290–3314.
31. J. Gong and A.J. Wilkinson: *Acta Mater.*, 2009, vol. 57, pp. 5693–5705.
32. J. Gong and A.J. Wilkinson: *Philos. Mag.*, 2011, vol. 91, pp. 1137–49.
33. W. Roberts, J. Gong, A.J. Wilkinson, and E. Tarleton: *Scripta Mater.*, 2020, vol. 178, pp. 119–23.
34. J.A. Medina Perilla and J.G. Sevillano: *Mater. Sci. Eng. A*, 1995, vol. 201, pp. 103–10.
35. J.J. Fundenberger, M.J. Philippe, F. Wagner, and C. Esling: *Acta Mater.*, 1997, vol. 45, pp. 4041–55.
36. R.A. Lebensohn and G.R. Canova: *Acta Mater.*, 1997, vol. 45, pp. 3687–94.
37. S. Ankem and H. Margolin: *Metall. Trans. A*, 1986, vol. 17, pp. 2209–26.
38. S. Suri, G.B. Viswanathan, T. Neeraj, D.H. Hou, and M.J. Mills: *Acta Mater.*, 1999, vol. 47, pp. 1019–34.
39. S. Zherebtsov, G. Salishchev, and S.L. Semiatin: *Philos. Mag. Lett.*, 2010, vol. 90, pp. 903–14.
40. D. Bhattacharyya, G.B. Viswanathan, R. Denkenberger, D. Furrer, and H.L. Fraser: *Acta Mater.*, 2003, vol. 51, pp. 4679–91.
41. T. Furuhashi, J.M. Howe, and H.I. Aaronson: *Acta Metall. Mater.*, 1991, vol. 39, pp. 2873–86.
42. R. Shi, N. Ma, and Y. Wang: *Acta Mater.*, 2012, vol. 60, pp. 4172–84.
43. W.H. Miller, R.T. Chen, and E.A. Starke: *Metall. Trans. A*, 1987, vol. 18, pp. 1451–68.
44. J.C. Williams and G. Luetjering: *Warrendale, PA: AIME* 1981, p. 671.
45. D.M. Bowden and E.A. Starke: *Metall. Trans. A*, 1984, vol. 15, pp. 1687–98.
46. K.S. Chan, C.C. Wojcik, and D.A. Koss: *Metall. Trans. A*, 1981, vol. 12, pp. 1899–1907.
47. Y. Mine, Y. Matsuzaki, and K. Takashima: *Scripta Mater.*, 2020, vol. 177, pp. 223–28.
48. Y. Htwe, K. Kwak, D. Kishi, Y. Mine, R. Ding, P. Bowen, and K. Takashima: *Mater. Sci. Eng. A*, 2018, vol. 715, pp. 315–19.
49. M.F. Savage, J. Tatalovich, and M.J. Mills: *Philos. Mag.*, 2004, vol. 84, pp. 1127–54.
50. M.F. Savage, J. Tatalovich, M. Zupan, K.J. Hemker, and M.J. Mills: *Mater. Sci. Eng. A*, 2001, vol. 319, pp. 398–403.
51. R. Ding, Y. Chiu, I.P. Jones, N. Escalé, F. Pettinari-Sturmell, and J. Douin: *J. Electron Microsc.*, 2011, vol. 61, pp. 31–36.
52. M.M.S. Gosh, S. Rokhlin, V. Sinha, W. Soboyejo, and J. Williams: U.S. Department of Transportation Federal Aviation Administration, 2007.
53. A. Ambard, L. Guétaz, F. Louchet, and D. Guichard: *Mater. Sci. Eng. A*, 2001, vol. 319–321, pp. 404–08.
54. Y. Chong, T. Bhattacharjee, M.-H. Park, A. Shibata, and N. Tsuji: *Mater. Sci. Eng. A*, 2018, vol. 730, pp. 217–22.
55. I. Sen, S. Roy, and M.F.X. Wagner: *Adv. Eng. Mater.*, 2017, vol. 19, p. 1700298.
56. S.R. Kalidindi and S. Pathak: *Acta Mater.*, 2008, vol. 56, pp. 3523–32.
57. S. Pathak and S.R. Kalidindi: *Mater. Sci. Eng. R Rep.*, 2015, vol. 91, pp. 1–36.
58. D.K. Patel, H.F. Alharbi, H.F. Alharbi, and S.R. Kalidindi: *Acta Mater.*, 2014, vol. 79, pp. 108–16.
59. A. Castillo and S.R. Kalidindi: *Front. Mater.*, 2019, vol. 6, p. 136.
60. H.-J. Bunge: *Texture Analysis in Materials Science: Mathematical Methods*, Elsevier, Amsterdam, 2013.
61. S.J. Vachhani, R.D. Doherty, and S.R. Kalidindi: *Acta Mater.*, 2013, vol. 61, pp. 3744–51.
62. S. Pathak, J. Shaffer, and S. Kalidindi: *Scripta Mater.*, 2009, vol. 60, pp. 439–42.
63. H. Hertz: *Miscellaneous Papers*, Macmillan, London, 1896.
64. S. Pathak, D. Stojakovic, R. Doherty, and S.R. Kalidindi: *J. Mater. Res.*, 2009, vol. 24, pp. 1142–55.
65. I.P. Jones and W.B. Hutchinson: *Acta Metall.*, 1981, vol. 29, pp. 951–68.
66. M.F. Savage: *Microstructural and Mechanistic Study of Low Temperature Creep and Dwell Fatigue in Single Colony Alpha/Beta Titanium Alloys*, The Ohio State University, Columbus, 2000.
67. S. Mohan, A.L. Pilchak, and S.R. Kalidindi: *NIST Materials Data Repository*, 2021.
68. E. Merson, R. Brydson, and A. Brown: In *Journal of Physics: Conference Series*, IOP Publishing: 2008, p. 012020.
69. R.I. Jaffee and N.E. Promisel: *The Science, Technology and Application of Titanium: Proceedings of an International Conference Organized by the Institute of Metals, the Metallurgical Society of Aime, and the American Society for Metals in Association with*



- the Japan Institute of Metals and the Academy of Sciences, USSR, and Held at th.* Elsevier, 2013.
70. P. Wang, M. Todai, and T. Nakano: *J. Alloy. Compd.*, 2019, vol. 782, pp. 667–71.
71. K.W. Katahara, M.H. Manghani, and E.S. Fisher: *J. Phys.*, 1979, vol. 9, p. 773.
72. N.V. Skripnyak, A.V. Ponomareva, M.P. Belov, and I.A. Abrikosov: *Mater. Des.*, 2018, vol. 140, pp. 357–65.
73. J.Y. Kim, V. Yakovlev, and S.I. Rokhlin: *AIP Conf. Proc.*, 2002, vol. 615, pp. 1118–25.
74. H.W. Rosenberg: *The Science, Technology and Application of Titanium*, Elsevier, Amsterdam, 1970, pp. 851–59.
75. A.R. Castillo, A. Venkatraman, and S.R. Kalidindi: *Integr. Mater. Manuf. Innov.*, 2021, vol. 10, pp. 99–114.

**Publisher's Note** Springer Nature remains neutral with regard to jurisdictional claims in published maps and institutional affiliations.

Springer Nature or its licensor (e.g. a society or other partner) holds exclusive rights to this article under a publishing agreement with the author(s) or other rightsholder(s); author self-archiving of the accepted manuscript version of this article is solely governed by the terms of such publishing agreement and applicable law.